IEEE Copyright Notice

This work has been submitted to the IEEE for possible publication. Copyright may be transferred without notice, after which this version may no longer be accessible.

Learning Visually Interpretable Oscillator Networks for Soft Continuum Robots from Video

Henrik Krauss¹, Johann Licher², Naoya Takeishi³, Annika Raatz², Takehisa Yairi³

Abstract—Data-driven learning of soft continuum robot (SCR) dynamics from high-dimensional observations offers flexibility but often lacks physical interpretability, while modelbased approaches require prior knowledge and can be computationally expensive. We bridge this gap by introducing (1) the Attention Broadcast Decoder (ABCD), a plug-and-play module for autoencoder-based latent dynamics learning that generates pixel-accurate attention maps localizing each latent dimension's contribution while filtering static backgrounds. (2) By coupling these attention maps to 2D oscillator networks, we enable direct on-image visualization of learned dynamics (masses, stiffness, and forces) without prior knowledge. We validate our approach on single- and double-segment SCRs, demonstrating that ABCD-based models significantly improve multistep prediction accuracy: 5.7× error reduction for Koopman operators and 3.5× for oscillator networks on the two-segment robot. The learned oscillator network autonomously discovers a chain structure of oscillators. Unlike standard methods, ABCD models enable smooth latent space extrapolation beyond training data. This fully data-driven approach yields compact, physically interpretable models suitable for control applications.

Keywords: Modeling, Control, and Learning for Soft Robots, Visual Learning, Model Learning for Control, Representation Learning, Koopman Theory

I. INTRODUCTION

The ability to learn dynamical systems directly from highdimensional observations has recently transformed how we model and control complex robots. For example, Dynamic Mode Decomposition (DMD), Koopman operator theory, and deep learning-based embeddings enable data-driven discovery of latent dynamics without explicit modeling [1]–[4]. Koopman operator methods offer the advantage of providing a linear representation of nonlinear dynamics, which facilitates prediction and control using linear methods [1].

Using (coupled) oscillator networks to describe latent dynamics, on the other hand, has been shown to be a versatile, expressive low-order time sequence modeling approach that offers potential (though not often used) for interpretability [5]. Learning dynamics directly from video data is attractive for both methods, as it requires minimal setup (no markers, trackers, or complex post-processing), no

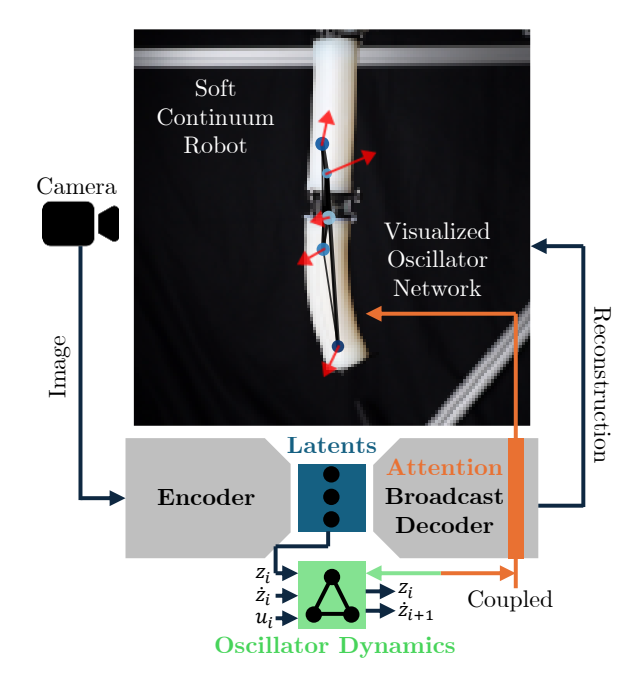


Fig. 1: Main contributions of this study: (1) A newly proposed attention broadcast decoder (ABCD) is used plugand-play for autoencoder-based Koopman and oscillator dynamics learning of a soft continuum robot. (2) Attention maps inside the ABCD are coupled to 2D oscillator dynamics so that the oscillator network can be visualized (here, masses, stiffnesses and actuation forces) on the original, reconstructed, or predicted future images.

prior knowledge, and allows end-to-end learning. Building on this idea, Stölzle and Della Santina demonstrated that inputto-state stable coupled oscillator networks (CONs) can learn latent-space dynamics of soft continuum robots (SCRs) from generated video data and support model-based control [6].

SCRs are an especially challenging research platform due to their infinite-dimensional, highly nonlinear mechanics [7]. Even if accurate models exist, they are often too computationally expensive for real-time control. As a result, data-driven dynamics learning has become an increasingly important direction in soft robotics. Recent reviews highlight the growing trend toward learning-based dynamics models for robotic manipulation [8].

Overall, a trade-off exists between interpretability, performance, and modeling accuracy. Data-driven methods provide flexibility and simplicity but often lack interpretability and

¹Henrik Krauss is with Department of Advanced Interdisciplinary Studies, The University of Tokyo, Tokyo, 153-8904, Japan. henrikl.krauss@gmail.com

²Johann Licher and Annika Raatz are with the Institute of Assembly Technology and Robotics, Leibniz University Hannover, 30823 Germany. licher@match.uni-hannover.de

³Naoya Takeishi and Takehisa Yairi are with the Research Center for Advanced Science and Technology, The University of Tokyo, Tokyo, 153-8904, Japan.

physical meaning. Model-driven approaches are interpretable and physically meaningful but require extensive prior modeling and are computationally heavy. Hybrid methods offer a promising compromise but still rely on manually designed physics components. To the best of our knowledge, no existing approach is fully data-driven yet yields a compact, physically interpretable low-parameter model suitable for control of soft continuum robots.

In this work we address this gap by

- proposing a novel Attention BroadCast Decoder (ABCD) for autoencoder-based latent dynamics learning from image sequences (video). It assigns pixel-accurate attention maps for each latent, indicating the location of the latents in the image while fully filtering out the static background.
- 2) showing how the attention maps of the ABCD can be coupled with oscillator network learning to enable physically meaningful on-image visualization of a 2D oscillator network. This achieves unprecedented levels of interpretability of learned dynamics and identification of low-order dynamics without prior knowledge.

This denotes a novel approach for deriving an SCR model from video data without prior knowledge, exhibiting a level of physical structure and interpretability similar to manual models.

II. RELATED WORK

A. Hybrid and Data-Driven Modeling of SCRs

Koopman-based models lift the nonlinear dynamics of soft continuum robots to a linear control space enabling real-time model predictive control (MPC) [9], [10]. Haggerty et al. [11] showed that Koopman methods can even be used to control highly dynamic motions of soft continuum robots. Ristich et al. [12] introduced a hybrid Koopman approach that improves simulation accuracy from small datasets by additionally using phase-space information from a Cosserat rod model.

Physics-informed neural networks (PINNs) combine physical priors and data for highly flexible yet structured learning. Liu et al. [13] use Lagrangian and Hamiltonian neural networks to control a tendon-driven SCR in simulation; however, real-robot results remain limited to quasi-static predictions due to the simplified underlying physics model. Licher et al. [14] train a domain-decoupled PINN [15] on a full Cosserat rod model and utilize it for adaptive MPC and state estimation.

Reduced-order modeling (ROM) methods also play a significant role in SCR modeling. Alkayas et al. [16] propose a structure-preserving autoencoder for fast simulation and control; in related work [17], an optimal strain parameterization based on proper orthogonal decomposition is introduced. These methods reduce system dimensionality while retaining essential physical structure.

Each of these methods has limitations: Koopman-based models do not offer a direct mechanistic interpretation, PINNs require manual derivation of physics models, and ROMs depend on accurate high-fidelity simulations that must also be derived by hand.

B. Vision-Based and Image-Driven Modeling of Soft Robots

Recent progress in vision-based learning highlights the potential of image-only sensing for soft robots. Zheng et al. [18] achieved online estimation of key points for multiple SCRs using stereo images and convolutional neural networks (CNNs). Rong and Gu [19] used CNNs for real-time shape estimation of self-occluding soft parallel robots. Almanzor et al. [20] utilized a CNN as a deep visual inverse-kinematics model for static shape control.

To also consider dynamics, Monteiro et al. [21] developed a visuo-dynamic self-modeling approach using recurrent networks, which learns from actuation inputs and video data to predict and control the motion of soft robots. A more interpretable hybrid model is presented by Valadas et al. [22], who learn a piecewise-constant strain model from video data and integrate it into a model-based controller.

None of these vision-based methods directly yields a compact and physically interpretable dynamical model. The approach of Stölzle and Della Santina [6] comes closest, yet their oscillators are not linked to the robot's physical configuration or structural elements, and the method is only demonstrated on simulated SCRs.

III. METHODS

A. Autoencoder-Based Latent Dynamics Learning

We implement an autoencoder-based latent dynamics learning approach for either Koopman or oscillator network learning based on and modified from [2], [6].

Given an input image $o^{(i)} \in \mathbb{R}^{c \times h \times w}$ at time step i, we extract the latent coordinate

$$\boldsymbol{z}^{(i)} = \varphi(\boldsymbol{o}^{(i)}) \in \mathbb{R}^k \tag{1}$$

with the encoder network φ . We then predict the next latent coordinate

$$z^{(i+1)} = f_{\text{dyn}}(z^{(i)}, \dot{z}^{(i)}, u^{(i)})$$
 (2)

after time interval Δt with the dynamical model $f_{\rm dyn}$, with φ and φ^{-1} being approximated by neural networks. We can then retrieve the predicted next image

$$\hat{o}^{(i+1)} = \varphi^{-1}(z^{(i+1)}) \tag{3}$$

with the decoder network φ^{-1} . This approach is similar to [2].

The latent velocities $\dot{z}^{(i)}$ together with the latent coordinates $z^{(i)}$ form the latent state. The latent velocities are obtained by mapping observation-space velocities to latent space via the encoder's Jacobian after [6]. Observation velocities are approximated using central finite differences which are then mapped to latent velocities using forward-mode automatic differentiation (AD)

$$\dot{\boldsymbol{z}}^{(i)} = \frac{\partial \varphi}{\partial \boldsymbol{o}}(\boldsymbol{o}^{(i)}) \cdot \dot{\boldsymbol{o}}^{(i)} \tag{4}$$

where $\partial \varphi/\partial o$ is the Jacobian of the encoder network evaluated at $o^{(i)}$.

We use a β -VAE [23] for the encoder and decoder networks. Following [2], the model is trained end-to-end with the basic loss

$$\mathcal{L}_{\text{basic}} = \frac{1}{N} \sum_{i=1}^{N} \left[\underbrace{\text{MSE}(\varphi^{-1}(\boldsymbol{z}^{(i)}), \boldsymbol{o}^{(i)})}_{\text{static reconstruction}} + \lambda_{\text{d}} \underbrace{\text{MSE}(\varphi^{-1}(\hat{\boldsymbol{z}}^{(i+1)}), \boldsymbol{o}^{(i+1)})}_{\text{dynamic reconstruction}} + \beta \left(-\frac{1}{2} \sum_{j} (1 + \log(\sigma_{j}^{(i)})^{2} - (\mu_{j}^{(i)})^{2} - (\sigma_{j}^{(i)})^{2}) \right) \underbrace{\text{KL divergence}}_{\text{KL divergence}} + \lambda_{z} \underbrace{\left(\text{MSE}(\hat{\boldsymbol{z}}^{(i+1)}, \boldsymbol{z}^{(i+1)}) + \text{MSE}(\Delta t \cdot \hat{\boldsymbol{z}}^{(i+1)}, \Delta t \cdot \hat{\boldsymbol{z}}^{(i+1)}) \right)}_{\text{latent dynamics consistency}} \right],$$
(5)

for a batch of size N, where $\sigma_j^{(i)}$ and $\mu_j^{(i)}$ are the standard deviation and mean of the j-th latent dimension $z_j^{(i)}$ of $z^{(i)}$. Additional losses as described below and in Sec. III-B are added inside \sum_i^N depending on network configuration.

For f_{dyn} , we employ both Koopman operators and oscillator networks:

Koopman dynamics: We learn a Koopman operator on the latent state $\boldsymbol{\xi}^{(i)} = [\boldsymbol{z}^{(i)\top}, \boldsymbol{\dot{z}}^{(i)\top}]^{\top}$ with learnable transition matrix $\boldsymbol{A} \in \mathbb{R}^{2k \times 2k}$ and feed-forward neural network (FNN) $\boldsymbol{B}(\cdot)$. The update is given by

$$\boldsymbol{\xi}^{(i+1)} = A\boldsymbol{\xi}^{(i)} + B(\boldsymbol{u}^{(i)}). \tag{6}$$

Oscillator network: We use learnable positive-definite mass M (diagonal), stiffness K, and Rayleigh damping matrices $D = \alpha M + \beta K$ with learnable $\alpha, \beta \geq 0$. The dynamics are governed by

$$M\ddot{z}^{(i)} + D\dot{z}^{(i)} + K(z^{(i)} - z_0) = B(u^{(i)}).$$
 (7)

Symplectic Euler integration is used during training for stability. For oscillator networks, we augment $\mathcal{L}_{\text{basic}}$ with a steady-state loss $\lambda_{\text{s}}\mathcal{L}_{\text{s}}$ to enforce $z^{(i)}=z_0$ and $\dot{z}^{(i)}=\mathbf{0}$ at equilibrium, encouraging physically consistent steady-state dynamics.

B. Attention Broadcast Decoder

1) Architecture: We introduce the Attention Broadcast Decoder (ABCD) as a plug-and-play module for autoencoder-based latent dynamics learning. It is inspired by the spatial broadcast decoder of Watters et al. [24], originally proposed for disentangled representation learning. As shown in Fig. 2(a), the ABCD takes latent coordinates $z^{(i)}$ and produces reconstructed images and pixel-accurate attention maps. It shall be noted that while the ABCD is used as a replacement for a standard CNN decoder, the ABCD implicitly affects the structure of the latent state and the dynamics model.

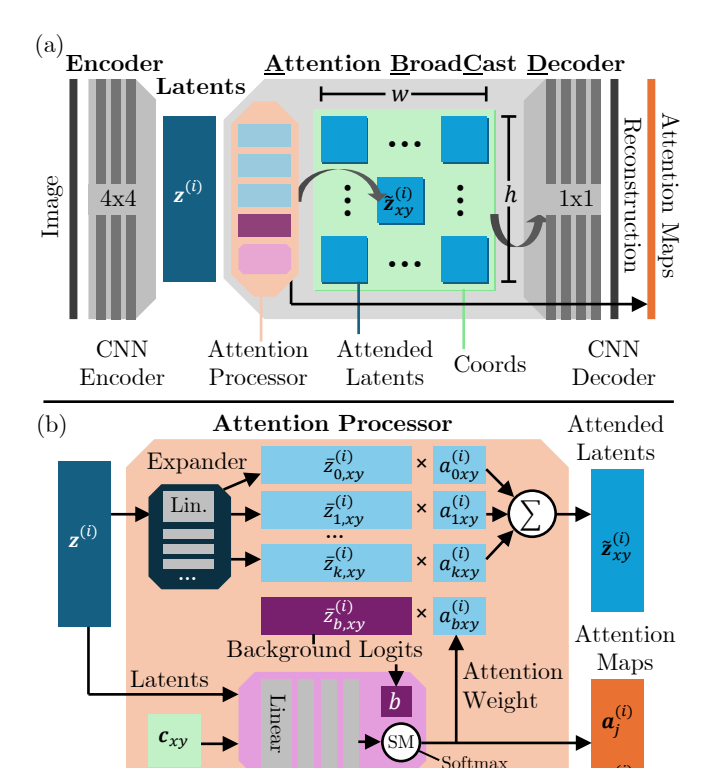


Fig. 2: (a) The attention broadcast decoder (ABCD) integrated plug-and-play in an autoencoder setup for image-reconstruction learning. (b) The attention processor within the ABCD that retrieves attention maps and attended latents before they are spatially broadcasted and decoded.

Attention Network

The attention processor (Fig. 2(b)) computes attended latents as follows: An FNN f_{att} produces attention logits

$$\ell_j^{(i)}(x,y) = f_{\text{att}}([\mathbf{z}^{(i)}, \mathbf{c}_{xy}])_j$$
 (8)

evaluating the latent coordinate $z^{(i)}$ at each coordinate pair $c_{xy} \in [-1,1]^2$. Pixel-wise attention values at location (x,y)

$$a_{j}^{(i)}(x,y) = \text{softmax}([\ell_{1}^{(i)}(x,y), \dots, \ell_{k}^{(i)}(x,y), b])_{j}, \quad (9)$$

are calculated by concatenating the logits with a constant background logit $b \equiv \ell_{k+1}^{(i)}(x,y)$ (a hyperparameter) and normalizing via softmax, resulting in attention maps $a_j^{(i)} \in \mathbb{R}^{h \times w}$ for $j=1,\ldots,k+1$, including the background attention map $a_b^{(i)}$. Optionally, adaptive Gumbel noise—controlled by a gumbel noise strength parameter—can be added to the logits before the softmax to encourage sharper, more competitive attention during training. Separately, each scalar latent $z_j^{(i)}$ is expanded to extended latents

$$\overline{\boldsymbol{z}}_{j,xy}^{(i)} = \boldsymbol{W}_j \boldsymbol{z}_j^{(i)} + \boldsymbol{b}_j \in \mathbb{R}^{n_f}, \tag{10}$$

via a linear layer of parameters W_j and b_j , mapping to feature width n_f and then broadcasted to image resolution, yielding $\overline{z}_j^{(i)} \in \mathbb{R}^{n_f \times h \times w}$. Additionally, learnable spatial background features $\overline{z}_b \in \mathbb{R}^{n_f \times h \times w}$ provide an auxiliary

expanded feature vector for capturing static background content. The attention-weighted latent coordinate maps are then computed by

$$\tilde{\boldsymbol{z}}^{(i)} = \sum_{j=1}^{k} \boldsymbol{a}_{j}^{(i)} \odot \overline{\boldsymbol{z}}_{j}^{(i)} + \boldsymbol{a}_{b}^{(i)} \odot \overline{\boldsymbol{z}}_{b}. \tag{11}$$

where \odot denotes element-wise multiplication. These are concatenated with coordinates and processed by four 1×1 CNN layers to construct the output image. Unlike the original spatial broadcast decoder [24] with the latent state uniformly broadcasted on the image resolution before final encoding, our approach makes individual latents compete for reconstruction of every output image pixel via the attention maps, i.e., yielding attention maps for each latent and background that show its relative contribution to the reconstruction of each pixel. Additionally, the introduced learnable background features allow to fully decouple the static background reconstruction from the latent state.

2) Attention consistency loss: While the ABCD can be used as described in Sec. III-B.1, we introduce an additional attention consistency loss

$$\mathcal{L}_{\text{attn-cons}} = \frac{1}{khw} \sum_{j=1}^{k} \sum_{x,y} \left| \dot{a}_{j}^{(i)}(x,y) \right| \cdot \left(1 - \dot{\bar{o}}^{(i)}(x,y) \right), \tag{12}$$

to regularize the attention dynamics, where $\dot{a}_{j}^{(i)}(x,y)$ is the time derivative (velocity) of the attention map for latent j at spatial location (x,y), computed via a Jacobian-vector product that propagates the observation velocity through the attention mechanism. Further, $\dot{o}^{(i)}(x,y)$ is the normalized velocity of the observation at pixel (x,y). This loss penalizes changes in the attention map at locations where the underlying image does not change, thereby encouraging the model to assign dynamic attention only to non-static regions. This creates a sharper transition between background and attention maps and stronger aligns attention dynamics with image dynamics.

3) 2D oscillator networks and attention coupling: For oscillator network learning when used with the ABCD, we introduce an additional modification that interprets the learned dynamics as a 2D oscillator network coupled to the attention maps to enable on-image visualization. We group consecutive pairs of latent dimensions into n=k/2 two-dimensional oscillators, where oscillator $l \in \{1,\ldots,n\}$ has latent-space position $q_l^{(i)} = [z_{2l-1}^{(i)}, z_{2l}^{(i)}]^{\top} \in \mathbb{R}^2$ and velocity $\dot{q}_l^{(i)} = [\dot{z}_{2l-1}^{(i)}, \dot{z}_{2l}^{(i)}]^{\top} \in \mathbb{R}^2$. We modify the ABCD's attention processor to generate one attention map $a_l^{(i)} \in \mathbb{R}^{h \times w}$ per oscillator (instead of per individual latent dimension). Correspondingly, the mass matrix M is constrained such that $M_{2l-1,2l-1} = M_{2l,2l}$ for all l, ensuring equal mass for both dimensions of each 2D oscillator, while the damping and stiffness matrices D and K remain unconstrained. To identify oscillator positions into image space, we compute

the center-of-mass (COM) of the squared attention maps:

$$\boldsymbol{p}_{l}^{(i)} = \frac{\sum_{x,y} (a_{l}^{(i)}(x,y))^{2} \cdot \boldsymbol{c}_{xy}}{\sum_{x,y} (a_{l}^{(i)}(x,y))^{2}} \in [-1,1]^{2}, \quad (13)$$

where $c_{xy} = [x,y]^{\top}$ are normalized pixel coordinates and squaring emphasizes regions of low mutual attention overlap, acting as a soft indicator of individual oscillator localization. The COM velocity $\dot{p}_l^{(i)}$ is computed via the quotient rule by propagating $\dot{o}^{(i)}$ through the attention mechanism using forward-mode AD. To ensure consistency between latent-space and image-space dynamics, we introduce an *attention coupling loss* that enforces matching pairwise relative motions:

$$\mathcal{L}_{\text{attn-coupling}} = \mathbb{E}_{l,m \neq l} \left[\left(\frac{\dot{d}_{lm}^{\text{lat}}(i)}{\bar{v}_{lm}^{\text{lat}}(i)} - \frac{\dot{d}_{lm}^{\text{img}}(i)}{\bar{v}_{lm}^{\text{img}}(i)} \right)^{2} \right], \quad (14)$$

where $\dot{d}_{lm}^{\rm lat}(i)$ and $\dot{d}_{lm}^{\rm img}(i)$ denote the signed relative velocities between oscillators l and m projected along their connecting direction in latent space $(\boldsymbol{q}_l, \boldsymbol{q}_m)$ and image space $(\boldsymbol{p}_l, \boldsymbol{p}_m)$, respectively, and $\bar{v}_{lm}(i)$ is the mean velocity magnitude of each pair. This approach assumes that distances in the image are proportional to the physical distances between the corresponding points on the robot.

C. Soft Continuum Robot Datasets

For this study the dynamic motion of one SCR with a single segment and one SCR consisting of two sequential connected by a rigid connector are investigated. The segments are soft pneumatic actuators with an outer diameter of $42.4\,\mathrm{mm}$ and a length of $130\,\mathrm{mm}$. They entail three fiber-reinforced pneumatic chambers arranged at 120° intervals around an inner channel. The actuator's main body is molded from EcoFlex 00-50 silicone (Smooth-On), while the base and tip caps are fabricated from Dragon Skin 30 silicone (Smooth-On). These actuators, in general, can generate spatial motion. However, only planar motion can be observed by a single camera. To ensure that the actuator only moves in a plane perpendicular to the camera axis, two of the actuator's chambers are connected to the same valve and therefore always hold the same pressure. We used 5/3 proportional valves (Enfield, LS-V05s) and absolute pressure sensors (First Sensor, 142BC30A-PCB), to control at 1 kHz using a PID controller implemented in Simulink. Further information about the actuator design and manufacturing as well as the pressure control setup are given in [25]. The video is recorded using a Sony Alpha 7 IV camera at 120 fps in Full HD.

To generate diverse motions covering the full workspace and a wide spectrum of frequencies, 75 pressure trajectories with randomly sampled frequencies from $0.04\,\mathrm{Hz}$ to $2\,\mathrm{Hz}$ and random phase shifts are generated. Each trajectory consists of two superposed frequencies. These $10\,\mathrm{s}$ -long trajectories are concatenated with a $2\,\mathrm{s}$ -long linear interpolated transition in between, which results in an overall duration of $15\,\mathrm{min}$. The linear interpolation reduces the excitation of natural oscillations, which would bury the controlled oscillation.

The dataset will be made publicly available¹.

IV. RESULTS

A. Neural Network Training Setup

All models are implemented in PyTorch and four configurations for each dataset are trained: (1) Koopman with standard decoder, (2) Koopman with ABCD ($+\mathcal{L}_{attn-cons}$), (3) 1D oscillator network with standard decoder, and (4) 2D oscillator network with coupled ABCD ($+\mathcal{L}_{attn-cons}$, $+\mathcal{L}_{attn-coupling}$). Images are downscaled to $3 \times 32 \times 32$ pixels and subsampled to 60 fps ($\Delta t = 1/60$ s). We use a latent dimension of k = 8for the 1-segment dataset (four 2D oscillators) and k = 10for the 2-segment dataset (five 2D oscillators). We train all models for 300 epochs using AdamW with a batch size of 32 and separate learning rates for encoder, dynamics, and decoder. For ABCD models, we employ a 5-epoch warmup phase with decreased encoder and dynamic model learning rate to encourage background information to be captured by the learnable background parameters of the decoder. Training is terminated early at 150 epochs (1-segment) and 100 epochs (2-segment) for the 2D oscillator networks with the ABCD, as we observe better generalization. The implementation including the detailed architecture, hyperparameters, loss weights, and training schedules is available on GitHub². A video containing animations of the results presented in Sec. IV-B-IV-D is provided as supplemental media and is also available on YouTube³.

B. Attention Maps

Fig. 3 shows the attention maps for the 1-segment and 2-segment robots for Koopman and oscillator networks using the ABCD, visualizing the relative contribution of each latent dimension to the reconstruction of each pixel or to the static background. We can see that all models accurately identify the static background, with a continuous gradient at the base of the SCR from latent attention maps to background map. The latent attention maps focus on different regions of the robots, showing the different information of the robot they encode. By visualizing the COM of the squared attention maps for the 2D oscillators, we can also see that they are distributed along the main axis of the 1-segment and 2-segment SCR.

C. On-Image Oscillator Networks

Figure 4 shows the learned 2D oscillator networks visualized on the robot images for both current and future states (20 steps ahead). Oscillator masses are represented by marker size, pairwise stiffness by line width, and current actuation forces by arrow length and direction. Markers are colored in different shades of blue to enable identification of the same oscillators in the corresponding latent space visualization shown on the right. The relative positions of the oscillator

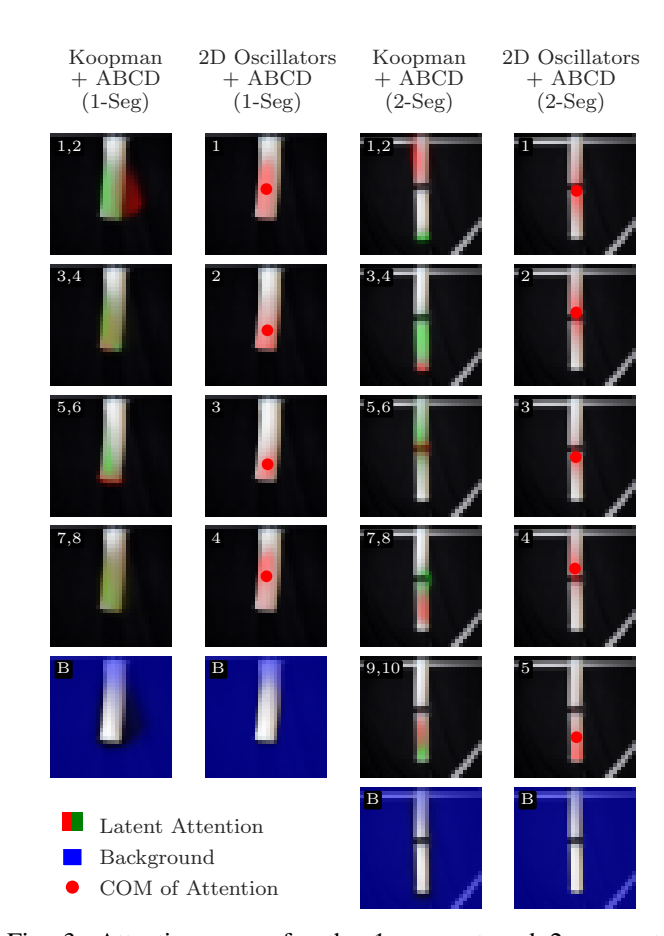


Fig. 3: Attention maps for the 1-segment and 2-segment robots for Koopman and oscillator networks using the ABCD. Two attention maps are shown per image for the Koopman models, to achieve visual compactness.

COMs in image space match their relative positioning when latents are interpreted as 2D coordinates in latent space, as enforced by the attention coupling loss $\mathcal{L}_{\text{attn-coupling}}$. It is noted that ground stiffness and damping are not visualized to avoid visual clutter.

For the 1-segment robot, the on-image visualization clearly demonstrates the high interpretability of the coupled oscillator network: internal forces push the robot to the left in the current state, and the future state indeed shows the robot moving leftward. For the 2-segment robot, the visualization reveals more complex dynamics. In the current state, one internal force pushes strongly to the right at the upper segment while the lower oscillators experience rightward forces. Correspondingly, the future state shows the upper segment bending left while the lower segment's curvature inverts to the right, accurately predicting the physical deformation.

Notably, the learned structure for the 2-segment robot forms a chain of five oscillators, which is physically meaningful: In Cosserat rod theory, soft continuum robots are represented by an infinite chain of coupled oscillators, and the ABCD-based oscillator network correctly identifies a finite chain as an accurate reduced-order approximation.

¹The dataset will be released publicly on Zenodo. A link will be added in a future revision.

²Code available at: https://github.com/UThenrik/visual_ oscillators_for_SCR

³Video available at: https://youtu.be/nbGgmY9bI-w



Fig. 4: On-image 2D oscillator networks for the 1-segment and 2-segment robots (left) and latent space visualization (right). A validation state (current) is shown as well as a future state, 20 steps ahead. The oscillator networks which accurately capture the SCR dynamics, are shown with their masses, stiffness, and current actuation forces. Oscillator positions are scaled 1.5 times around their shared mean position and higher resolution images are used for visual clarity.

The spatial distribution of oscillators is also insightful: two oscillators at each end are spread out along the robot, while three middle oscillators cluster near the connecting segment and exhibit high mutual stiffness. This structure aligns with the physical construction, as the two-segment robot is connected by a stiff intermediate element.

D. Single and Multi-Step Prediction

We evaluate all trained networks on single-step and multistep prediction tasks on validation trajectories. We initialize each model with an observation and its latent velocity (computed via central differences and forward-mode AD), then autoregressively predict the next 30 steps $(0.5\,\mathrm{s})$ by repeatedly applying the learned dynamics. Prediction errors denote the dynamic reconstruction loss, averaged over 50 randomly sampled validation trajectories per model. Single-step errors represent the MSE of the first predicted frame, while multi-step errors are averaged over all 30 prediction steps.

Fig. 5 shows the reconstruction error over time and steps for both 1-segment and 2-segment robots and Fig. 6 shows the reconstruction images. For the 1-segment robot, all models achieve similar single-step and multi-step errors, apart from the 2D oscillator network with coupled ABCD which has a higher single-step prediction error and slightly higher multi-step error. Though looking at the reconstructed images in Fig. 6, all models sufficiently accurately predict the 1-segment robot dynamics. For the more complex 2-segment robot, the performance differences are more pronounced:

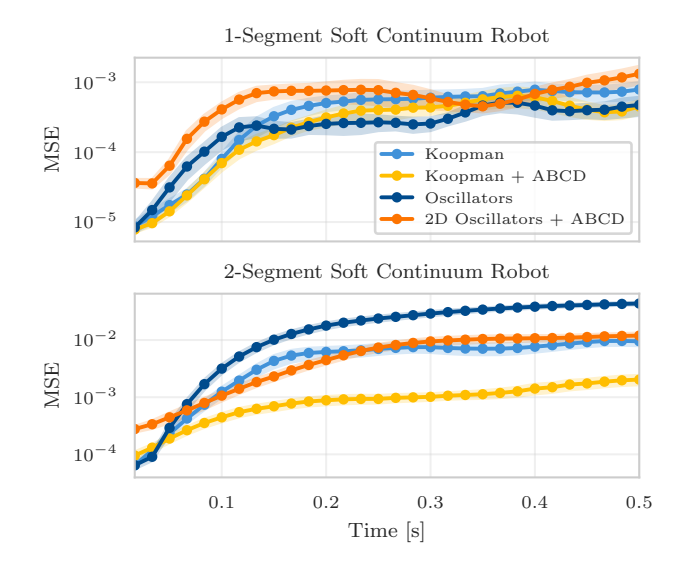


Fig. 5: Multi-step reconstruction error over $0.5\,\mathrm{s}$ for 1-segment (top) and 2-segment (bottom) robots. Shaded regions indicate standard error of the mean over 50 validation trajectories. The ABCD improves multi-step reconstruction accuracy for the more complex 2-segment system for both Koopman and oscillator network dynamics.

Koopman with ABCD achieves the best multi-step reconstruction error of 9.84×10^{-4} , significantly outperforming the standard Koopman (5.66×10^{-3}) , while the 2D oscillator network with ABCD (6.56×10^{-3}) also outperforms the

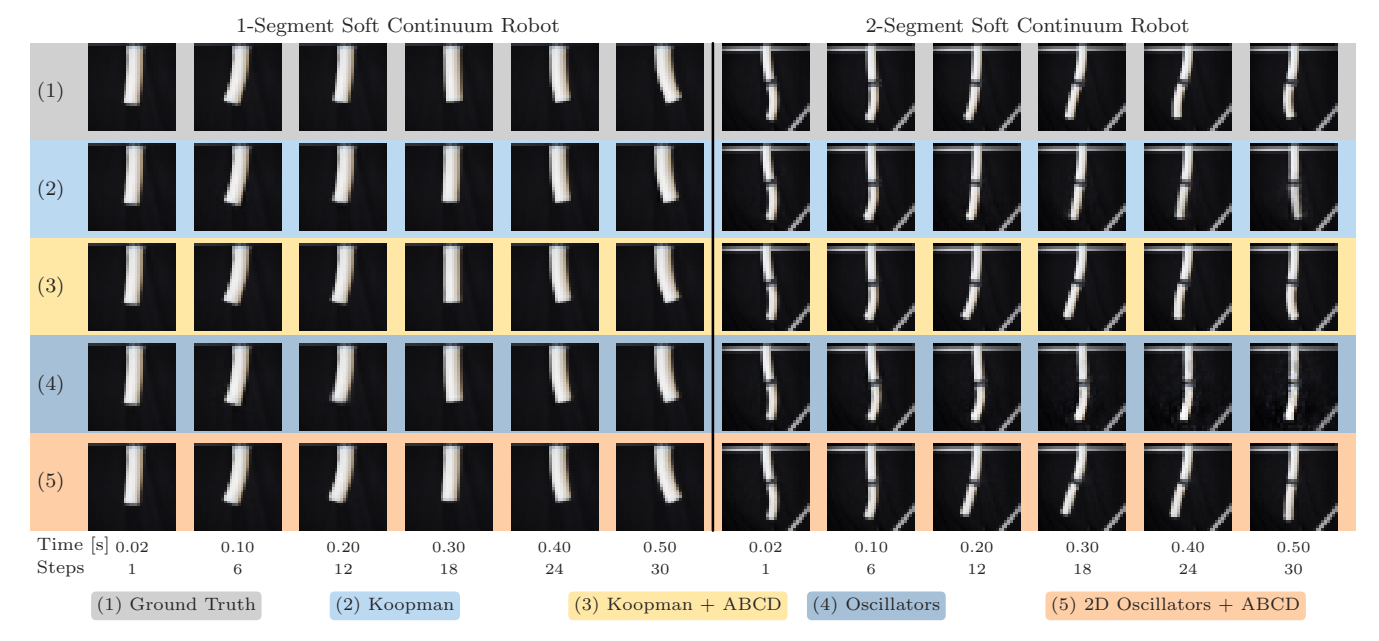


Fig. 6: Multi-step reconstruction images (single step and every 6th step shown) over $0.5\,\mathrm{s}$ for 1-segment and 2-segment robots compared to ground truth for a validation trajectory. All 1-segment networks achieve highly accurate reconstructions. For the 2-segment robot, the ABCD improves long-term reconstruction accuracy for both Koopman and oscillator network dynamics.

standard oscillator network (2.27×10^{-2}) . The networks using the ABCD have slightly worse single-step reconstruction errors. However, we can observe sufficiently accurate single-step reconstructions in Fig. 6 and more accurate multi-step reconstructions for the networks using the ABCD, where the plain Koopman and oscillator networks diverge.

E. Latent Space Extrapolation

To evaluate the learned latent representations' ability to extrapolate observed trajectories, we perform linear interpolation and extrapolation in latent space. We select two latent states from the data set, separated by 10 time steps, representing a transition of the robot from a left-bent configuration to an approximately neutral position. For extrapolation factors $\alpha \in \{1.2, 1.5, 2, 3\}$, we compute $\mathbf{z}_{\text{extra}} = \mathbf{z}^{(i)} + \alpha(\mathbf{z}^{(i+10)} - \mathbf{z}^{(i)})$ and decode the extrapolated latent states.

Fig. 7 reveals a significant difference between models with and without the ABCD. Both Koopman with ABCD and the 2D oscillator network with coupled ABCD successfully extrapolate the bending movement, with a transition from the left-to-right bending motion, beyond a bending angle that is represented in the dataset (for $\alpha=3$). In contrast, the standard Koopman and oscillator networks without ABCD decoder fail to generate a meaningful extrapolation: their reconstructions become trapped at the near-neutral configuration and produce noisy images. This indicates that the attention mechanism not only improves interpretability and multi-step prediction accuracy for the 2-segment SCR but also learns more structured latent representations. This is expected to be highly beneficial for control.

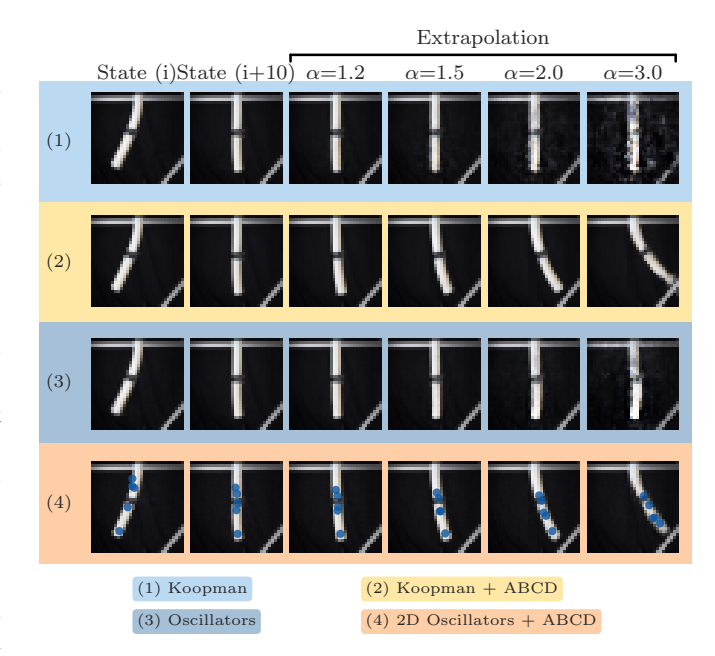


Fig. 7: Latent space extrapolation for 2-segment robot models. Two states 10 steps apart (left-bent and right-bent) are linearly extrapolated in latent space with factor α . Blue markers indicate oscillator positions for attention-based models. ABCD models successfully extrapolate a bending transitions from left to right, while standard models produce non-bent, noisy states.

V. CONCLUSIONS

This work introduced the Attention Broadcast Decoder (ABCD) for autoencoder-based latent dynamics learning from video, that is highly interpretable, accurate and computationally efficient. The ABCD generates pixel-precise attention maps for each latent dimension to enable spatial localization of learned features, and separates static background from dynamic robot motion. We demonstrated its plug-and-play integration with both Koopman operators and oscillator networks for dynamics learning of a single and double-segment soft continuum robot.

By coupling attention maps to 2D oscillator networks through an attention coupling loss, we enabled direct onimage visualization of learned dynamics, i.e., masses, stiffness, and forces, without prior knowledge of the system. For the 2-segment robot, the model autonomously discovered a chain structure consistent with Cosserat rod theory. The ABCD not only provides unprecedented interpretability but also significantly improves multi-step prediction accuracy for the complex 2-segment robot: 5.7 × error reduction for Koopman $(9.84 \times 10^{-4} \text{ vs. } 5.66 \times 10^{-3})$ and $3.5 \times \text{ for}$ oscillator networks (6.56 \times 10⁻³ vs. 2.27 \times 10⁻²). Both Koopman and oscillator network variants with ABCD further enable smooth latent space extrapolation where standard methods fail. Notably, only 4 and 5 2D oscillators are required for the 1- and 2-segment robot, respectively, denoting computationally efficient dynamics models.

The presented approach enables future work in several directions. Applications to control are promising, where the interpretable on-image visualizations may facilitate target state specification and trajectory planning. The learned matrices offer opportunities for parameter identification such as material specifications and simulation of structural modifications such as robot damage. The approach could be extended to different (soft) robotic systems, and to multi-camera setups, potentially learning 3D oscillator networks akin to finite element models. Additionally, transferring learned dynamics to different camera perspectives may be facilitated, as latents correspond to smoothly localized regions of the robot without encoding background information.

REFERENCES

- S. L. Brunton, M. Budišić, E. Kaiser, and J. N. Kutz, "Modern koopman theory for dynamical systems," *SIAM Review*, vol. 64, no. 2, pp. 229–340, 2022.
- [2] B. Lusch, J. N. Kutz, and S. L. Brunton, "Deep learning for universal linear embeddings of nonlinear dynamics," *Nature communications*, vol. 9, no. 1, p. 4950, 2018.
- [3] Y. Li, H. He, J. Wu, D. Katabi, and A. Torralba, "Learning compositional koopman operators for model-based control," in 8th International Conference on Learning Representations, ICLR 2020, Addis Ababa, Ethiopia, April 26-30, 2020. OpenReview.net, 2020.
- [4] N. Takeishi, Y. Kawahara, and T. Yairi, "Learning koopman invariant subspaces for dynamic mode decomposition," in *Advances in Neural Information Processing Systems*, I. Guyon, U. V. Luxburg, S. Bengio, H. Wallach, R. Fergus, S. Vishwanathan, and R. Garnett, Eds., vol. 30. Curran Associates, Inc., 2017.
- [5] S. Lanthaler, T. K. Rusch, and S. Mishra, "Neural oscillators are universal," in *Advances in Neural Information Processing Systems*, A. Oh, T. Naumann, A. Globerson, K. Saenko, M. Hardt, and S. Levine, Eds., vol. 36. Curran Associates, Inc., 2023, pp. 46786–46806.

- [6] M. Stölzle and C. Della Santina, "Input-to-state stable coupled oscillator networks for closed-form model-based control in latent space," in Advances in Neural Information Processing Systems, 2024.
- [7] C. Laschi, T. G. Thuruthel, F. Lida, R. Merzouki, and E. Falotico, "Learning-Based Control Strategies for Soft Robots: Theory, Achievements, and Future Challenges," *IEEE Control Systems Magazine*, vol. 43, no. 3, pp. 100–113, 2023.
- [8] B. Ai, S. Tian, H. Shi, Y. Wang, T. Pfaff, C. Tan, H. I. Christensen, H. Su, J. Wu, and Y. Li, "A review of learning-based dynamics models for robotic manipulation," *Science Robotics*, vol. 10, no. 106, p. eadt1497, 2025.
- [9] D. Bruder, X. Fu, R. B. Gillespie, C. D. Remy, and R. Vasudevan, "Data-Driven Control of Soft Robots Using Koopman Operator Theory," *IEEE Transactions on Robotics*, vol. 37, no. 3, pp. 948–961, 2021.
- [10] L. Shi, Z. Liu, and K. Karydis, "Koopman operators for modeling and control of soft robotics," *Current Robotics Reports*, vol. 4, no. 2, pp. 23–31, 2023.
- [11] D. A. Haggerty, M. J. Banks, E. Kamenar, A. B. Cao, P. C. Curtis, I. Mezić, and E. W. Hawkes, "Control of soft robots with inertial dynamics," *Science Robotics*, vol. 8, no. 81, p. eadd6864, 2023.
- [12] E. Ristich, L. Zhang, Y. Ren, and J. Sun, "Physics-Informed Split Koopman Operators for Data-Efficient Soft Robotic Simulation," in 2025 IEEE International Conference on Robotics and Automation (ICRA), 2025, pp. 9273–9279.
- [13] J. Liu, P. Borja, and C. Della Santina, "Physics-Informed Neural Networks to Model and Control Robots: A Theoretical and Experimental Investigation," *Advanced Intelligent Systems*, vol. 6, no. 5, p. 2300385, 2024
- [14] J. Licher, M. Bartholdt, H. Krauss, T.-L. Habich, T. Seel, and M. Schappler, "Adaptive model-predictive control of a soft continuum robot using a physics-informed neural network based on cosserat rod theory," 2025.
- [15] H. Krauss, T.-L. Habich, M. Bartholdt, T. Seel, and M. Schappler, "Domain-Decoupled Physics-informed Neural Networks with Closed-Form Gradients for Fast Model Learning of Dynamical Systems," in Proceedings of the 21st International Conference on Informatics in Control, Automation and Robotics. SCITEPRESS - Science and Technology Publications, 2024, pp. 55–66.
- [16] A. Y. Alkayas, A. T. Mathew, D. Feliu-Talegon, Y. Zweiri, T. G. Thuruthel, and F. Renda, "Structure-preserving model order reduction of slender soft robots via autoencoder-parameterized strain," *IEEE Robotics and Automation Letters*, vol. 10, no. 10, pp. 11006–11013, 2025.
- [17] A. Y. Alkayas, A. T. Mathew, D. Feliu-Talegon, P. Deng, T. G. Thuruthel, and F. Renda, "Soft synergies: Model order reduction of hybrid soft-rigid robots via optimal strain parameterization," *IEEE Transactions on Robotics*, vol. 41, pp. 1118–1137, 2025.
- [18] H. Zheng, S. Pinzello, B. G. Cangan, T. J. Buchner, and R. K. Katzschmann, "Vision-based online key point estimation of deformable robots," *Advanced Intelligent Systems*, vol. 6, no. 10, p. 2400105, 2024.
- [19] Y. Rong and G. Gu, "Vision-based real-time shape estimation of self-occluding soft parallel robots using neural networks," *IEEE Robotics and Automation Letters*, vol. 9, no. 8, pp. 7349–7356, 2024.
- [20] E. Almanzor, F. Ye, J. Shi, T. G. Thuruthel, H. A. Wurdemann, and F. Iida, "Static Shape Control of Soft Continuum Robots Using Deep Visual Inverse Kinematic Models," *IEEE Transactions on Robotics*, vol. 39, no. 4, pp. 2973–2988, 2023.
- [21] R. Marques Monteiro, J. Shi, H. Wurdemann, F. Iida, and T. George Thuruthel, "Visuo-dynamic self-modelling of soft robotic systems," Frontiers in Robotics and AI, vol. Volume 11 - 2024, 2024.
- [22] R. Valadas, M. Stölzle, J. Liu, and C. D. Santina, "Learning Low-Dimensional Strain Models of Soft Robots by Looking at the Evolution of Their Shape with Application to Model-Based Control," in 2025 IEEE 8th International Conference on Soft Robotics (RoboSoft), 2025, pp. 1–8.
 [23] I. Higgins, L. Matthey, A. Pal, C. Burgess, X. Glorot, M. Botvinick,
- [23] I. Higgins, L. Matthey, A. Pal, C. Burgess, X. Glorot, M. Botvinick, S. Mohamed, and A. Lerchner, "beta-vae: Learning basic visual concepts with a constrained variational framework," in *International* conference on learning representations, 2017.
- [24] N. Watters, L. Matthey, C. P. Burgess, and A. Lerchner, "Spatial broadcast decoder: A simple architecture for learning disentangled representations in vaes," arXiv preprint arXiv:1901.07017, 2019.
- [25] A. N., "Title blinded," in Conference X, 2021.